

# A Double-Sine-Gordon Early Universe

Behnoush Afshar<sup>1,\*</sup>, Marziyeh Peyravi<sup>2,†</sup>, Kazuharu Bamba<sup>3,‡</sup> and Hooman Moradpour<sup>1,§</sup>

<sup>1</sup> *Research Institute for Astronomy and Astrophysics of Maragha (RIAAM),  
University of Maragheh, P.O. Box 55136-553, Maragheh, Iran*

<sup>2</sup> *Department of Physics, School of Sciences, Ferdowsi University of Mashhad, 91775-1436, Mashhad, Iran*

<sup>3</sup> *Faculty of Symbiotic Systems Science, Fukushima University, Fukushima 960-1296, Japan*

A solitonic model of the early universe is introduced by employing the Double-Sine-Gordon (DSG) potential. The model predicts the appropriate number of e-foldings ( $N_e$ ) required for favored inflation and is an advantage for the model in addressing the flatness, horizon, and magnetic monopole problems. Compatibility of the model with observations, including the Planck 2018 data [1] and the Planck 2018 data+BK18+BAO [2] paves the way to estimate the model's free parameters. The results generate acceptable and proper values for the spectral index ( $n_s$ ) and the tensor-to-scalar ratio ( $r$ ) in agreement with the Planck 2018 data [1] and the Planck 2018 data+BK18+BAO [2]. Correspondingly, a consistent description of the reheating era is obtained, yielding positive reheating number of e-foldings ( $N_{\text{reh}}$ ) and reheating final temperature ( $T_{\text{reh}}$ ) from  $10^{-2}$  GeV to  $10^{16}$  GeV. Overall, the model seems viable at the inflationary and reheating eras.

## I. INTRODUCTION

Although the observation of the cosmic microwave background radiation (CMB [3]) shed light on the study of the dark ages of the cosmos [4], the CMB also seems beneficial to study other parts of the cosmos. As an example, the lensing of CMB photons leads us to study dark energy that is responsible for the current accelerating universe first reported by E. Hubble [5]. The flatness problem, as formulated by Dicke and Peebles [6, 7], rooted in the fine-tuned density of matter and energy in the early universe leading to the observed flatness on large-scale structures [4, 8–12], is one of the basic concerns in understanding the early universe. The explanation of the homogeneity and the thermal equilibrium of the CMB [4, 8–10], related to the horizon problem, forms another problem [13]. In addition, the magnetic monopole problem, first highlighted by Dirac [14], concerns the absence of magnetic monopoles despite theoretical predictions [4, 10, 11, 15]. To address the mentioned challenges, in 1981, Guth [16] introduced the concept of inflation as an exponentially expansion driven by a scalar field. In 1980, Starobinsky [17] had also proposed a different mechanism for inflation using gravitational effects. It is worthwhile mentioning that the relationship between the first-order phase transition of vacuum and the expansion of the universe has been studied by Sato [18]. Others later expanded and improved these studies [19–22].

Generally, inflation with the number of e-foldings ( $N_e$ ) in the range of 40 to 70 [9, 10, 23–31] reduces the initial curvature of the cosmos, finally solving the flatness problem [8–12]. Therefore, the homogeneity and the thermal equilibrium of the CMB rooted in the fact that these regions were in a causal relationship at the beginning of

inflation [8–11]. Moreover, inflation can dilute the density of magnetic monopoles, making them very difficult to detect [10, 11, 15]. It should also be noted that the idea of inflation not only overcomes the problems listed above, but it also has substantial experimental successes in predicting specific aspects of CMB fluctuations and provides a mechanism for the origin of large-scale structures [32, 33].

The reheating mechanism explains the transfer of energy stored in the inflaton field into the other degrees of freedom that finally heats the cosmos. This happens in a phase immediately following the primary inflationary era and is called the reheating era [11, 25, 28, 29, 31, 34–37]. Three parameters that describe this period are the reheating number of e-foldings  $N_{\text{reh}}$ , the reheating final temperature  $T_{\text{reh}}$ , and the reheating effective equation of state (EoS)  $\omega_{\text{reh}}$  [28, 29, 31, 36, 37]. The amount of expansion that happens between the end of inflation and the beginning of the radiation-dominated era is denoted by the reheating number of e-foldings  $N_{\text{reh}}$  [28, 29, 31, 36, 37].  $T_{\text{reh}}$  represents the energy of the particles created due to the reheating [25, 28, 36], and the minimum permissible  $T_{\text{reh}}$  is constrained by the fact that the temperature of Big Bang nucleosynthesis  $T_{\text{BBN}}$  cannot be less than  $10^{-2}$  GeV [28, 29, 31, 36, 37]. Furthermore, the maximum value of  $T_{\text{reh}}$  ( $T_{\text{reh,max}}$ ) depends entirely on the inflationary model [38–41]. The decay of inflaton field yields particles linked to the Grand Unified Theory (GUT) scale (an energy range of approximately  $10^{15}$  GeV to  $10^{16}$  GeV). At this energy scale, the weak nuclear force, the strong nuclear force, the electromagnetic force, and gravity coalesce into a unified force, and additionally, the temperatures  $T_{\text{reh,max}}$  and  $T_{\text{GUT}}$  exhibit close proximity [42].

The relationship between the pressure and energy density of the dominant fluid in the reheating phase is described by its EoS ( $\omega_{\text{reh}}$ ) [28, 29, 31, 36, 37]. In the inflationary era,  $\omega < -\frac{1}{3}$  is acceptable and  $\omega = -1$  is considered as most ideal state [43]. In this regard, it is useful to mention that the EoS parameters for cosmic

\* behnoush.afshar.cosmology@gmail.com

† marziyeh.peyravi@stu-mail.um.ac.ir

‡ bamba@sss.fukushima-u.ac.jp

§ hn.moradpour@maragheh.ac.ir

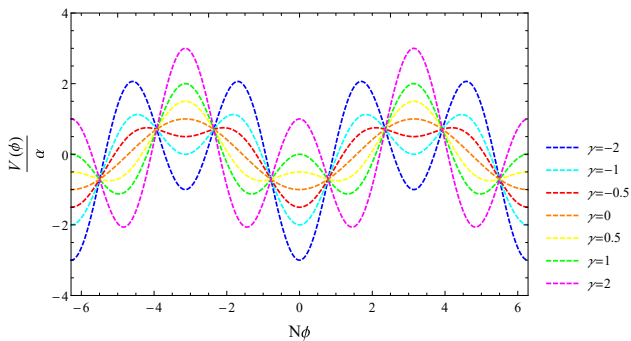


FIG. 1:  $\frac{V(\phi)}{\alpha}$  as a function of  $N\phi$  for  $\alpha > 0$  and several values of  $\gamma$ . Eq. (2) can be used to calculate the point with zero potential, while Eq. (5) represents extremum points of potential (1).

strings and domain walls are  $\omega = -\frac{1}{3}$  and  $\omega = -\frac{2}{3}$ , respectively [44]. Cosmic strings and domain walls might arise as the topological defects that occurred during a phase transition in the early universe [45]. Compared to the energy density of dust, its pressure is negligible and thus  $\omega = 0$  in the matter dominated era. On the other hand, radiation (an extremely relativistic source) meets  $\omega = \frac{1}{3}$  [46], and thus, particles with  $\omega > \frac{1}{3}$ , known as ultra-lights, have speeds exceeding that of light and have not been observed thus far [45].

Inflationary models usually contain scalar fields with high energy density, known as inflaton fields [47–49]. According to the simplest field theory, scalar fields interact only with gravitational interactions, but not with other matter or radiation [48, 50]. While GUT allows various solitonic structures, such as cosmic strings, magnetic monopoles and domain walls [51, 52], inflation reduces the number of these solitonic structures drastically [52, 53]. Therefore, it would be constructive to provide and study solitonic models of inflation. According to these ideas, studies have been conducted on inflation in the context of soliton fields [54–62]. The papers [54, 56, 59, 60, 62] presented natural inflation models with the pseudo-Nambu-Goldstone bosons (PNGBs) potential and evaluating their ability to agree observational data and produce suitable  $N_e$ . The mass inflation models [55], brane inflation [57, 58], as well as the relationship between inflationary models with dark energy and dark matter have also been studied [60, 61].

However, there is a lack of studies on reheating and agreement results with the Planck 2018 data [1] and the Planck 2018 data+BK18+BAO [2]. Solitonic models have also achieved remarkable success in the fields of string theory [63, 64], dark matter [60, 65–67], black holes [68, 69], and even gravitational waves [70–72]. Thus, a deeper knowledge of the early universe in the framework of solitonic models can shed light on these attempts as well as interactions between early universe and particle physics that finally opens up new perspectives on the dynamics and the evolution of the universe together with

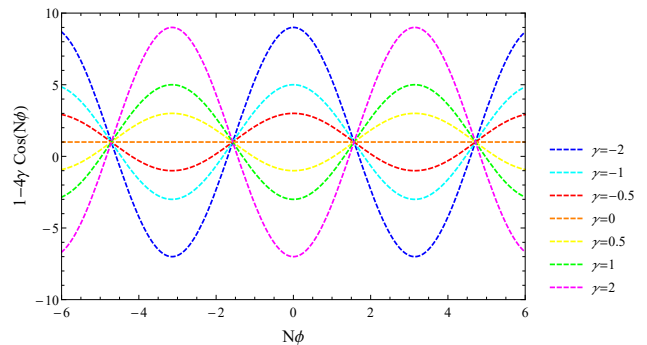


FIG. 2:  $1 - 4\gamma \cos(N\phi)$  as a function of  $N\phi$  for  $\alpha > 0$  and several values of  $\gamma$ . The sign of this function is used to specify different intervals in Table. I. It also plays a critical role in the value of Eq. (21), which represents  $N_e$ .

the formation of cosmic structures. This motivates us to examine the eras of inflation and reheating in the framework of the DSG potential.

The paper is organized as follows. Next section provides a brief overview of the DSG potential. In Sec. III, focusing on the scalar spectral index  $n_s$  and the tensor-to-scalar ratio  $r$  and by confronting the theory with the Planck 2018 data [1] and the Planck 2018 data+BK18+BAO [2], the permissible values of the free parameters of model are obtained. In this line, the ability of the model in achieving the number of e-foldings  $N_e$  from 30 to 55 is also investigated. The reheating era is also studied in the fourth section. A summary is finally provided at the last section. In this study, it is assumed that  $c = \hbar = 1$  and the reduced Planck mass is indicated by  $M_{\text{Pl}} = \sqrt{\frac{1}{8\pi G}} = 2.435 \times 10^{18}$  GeV.

## II. DOUBLE-SINE-GORDON POTENTIAL

Combining the harmonic term and the self-interaction of the PNGBs leads to the DSG potential [73–76]

$$V(\phi) = -\alpha \cos(N\phi) + \beta \cos(2N\phi), \quad (1)$$

in which  $\alpha$ ,  $\beta$  and  $N$  are free parameters, and  $\phi$  denotes the soliton field. For the sake of convenience, the ratio of  $\beta$  to  $\alpha$  is stored into parameter  $\gamma$  ( $\equiv \frac{\beta}{\alpha}$ ). In Fig. 1, we show the behavior of  $\frac{V(\phi)}{\alpha}$  for  $\alpha > 0$  and some values of  $\gamma$ . As mentioned in the following section,  $\alpha < 0$  lacked acceptable solutions and is hence not considered in this research.

As it is obvious from Fig. 1, one gets  $V(\phi) = 0$  when

$$N\phi = \begin{cases} \pm X + 2\pi m & \text{if } |\gamma| \geq 1 \\ \pm Y + 2\pi m & \end{cases} \quad m \in Z, \quad (2)$$

Interval	Sign of $V'(\phi)$	Sign of $(1 - 4\gamma \cos(N\phi))$	$N\phi$ Range for $-1 \leq \gamma$	$N\phi$ Range for $-1 < \gamma < 0$	$N\phi$ Range for $0 \leq \gamma < 1$	$N\phi$ Range for $1 \geq \gamma$
1	Positive	Positive	$Y + 2\pi m < N\phi < Z + 2\pi m$	$Y + 2\pi m < N\phi < Z + 2\pi m$	$Y + 2\pi m < N\phi < 2\pi(m + 0.5)$	$X < N\phi < 2\pi(m + 0.5)$
2	Negative	Negative	$Z + 2\pi m < N\phi < X + 2\pi m$	$Z + 2\pi m < N\phi < 2\pi(m + 0.5)$	None	$2\pi m < N\phi < Y + 2\pi m$
3	Positive	Negative	$-X + 2\pi(m + 1) < N\phi < -Z + 2\pi(m + 1)$	$2\pi(m + 0.5) < N\phi < -Z + 2\pi(m + 1)$	None	$-Y + 2\pi(m + 1) < N\phi < 2\pi(m + 1)$
4	Negative	Positive	$-Z + 2\pi(m + 1) < N\phi < -Y + 2\pi(m + 1)$	$-Z + 2\pi(m + 1) < N\phi < -Y + 2\pi(m + 1)$	$2\pi(m + 0.5) < N\phi < -Y + 2\pi(m + 1)$	$2\pi(m + 0.5) < N\phi < -X + 2\pi(m + 1)$

TABLE I: Four intervals of  $N\phi$  with  $V(\phi) > 0$  and  $\alpha > 0$  defined are based on the signs of  $V'(\phi)$  and  $(1 - 4\gamma \cos(N\phi))$ .

in which

$$X \cong \arccos\left(\frac{1 + \sqrt{1 + 8\gamma^2}}{4\gamma}\right), \quad (3)$$

and

$$Y \cong \arccos\left(\frac{1 - \sqrt{1 + 8\gamma^2}}{4\gamma}\right). \quad (4)$$

There are also four extremes obtained by

$$N\phi = \begin{cases} 2\pi m \\ Z + 2\pi m \\ 2\pi(m + 0.5) \\ -Z + 2\pi(m + 1) \end{cases} \quad m \in Z, \quad (5)$$

in which

$$Z \cong \arccos\left(\frac{1}{2\gamma}\right). \quad (6)$$

### III. INFLATION

In this section, the slow-roll inflation driven by the DSG potential (1) is discussed. For a homogeneous and isotropic universe, the Friedmann-Robertson-Walker (FRW) metric is written as

$$g_{\mu\nu} dx^\mu dx^\nu = -dt^2 + a(t)^2 \delta_{ij} dx^i dx^j, \quad (7)$$

where  $a$  is the scale factor and considered 0 at the start of Big Bang. The total action is expressed as

$$S_{tot} = S_g + S_\phi, \quad (8)$$

in which

$$S_g = M_{\text{Pl}}^2 \int d^4x \sqrt{-g} \left(\frac{R}{2}\right), \quad (9)$$

and

$$S_\phi = \int d^4x \sqrt{-g} \left[-\frac{1}{2} g^{\mu\nu} \partial_\mu \phi \partial_\nu \phi - V(\phi)\right], \quad (10)$$

denote the gravitational action and the soliton field term, respectively. Here,  $g = g_{\mu\nu} g^{\mu\nu}$ ,  $R = R_{\mu\nu} R^{\mu\nu}$  represents the Ricci scalar, and  $V(\phi)$  is the potential of the soliton field  $\phi$ . Using the total action (8), the Friedmann equations are achieved as

$$3M_{\text{Pl}}^2 H^2 = \frac{1}{2} \dot{\phi}^2 + V(\phi), \quad (11)$$

and

$$-M_{\text{Pl}}^2 (3H^2 + 2\dot{H}) = \frac{1}{2} \dot{\phi}^2 - V(\phi), \quad (12)$$

in which  $H = \frac{\dot{a}}{a}$  denotes the Hubble parameter, and dot indicates the time derivative. It is simple to demonstrate that Eqs. (11) and (12) lead to

$$\dot{H} = -\frac{M_{\text{Pl}}^2}{2} \dot{\phi}^2. \quad (13)$$

In addition, varying the total action (8) with respect to  $\phi$ , one finds

$$\ddot{\phi} + 3H\dot{\phi} + V'(\phi) = 0, \quad (14)$$

where  $V'(\phi) = \frac{dV(\phi)}{d\phi}$ . The Hubble slow-roll parameters are defined as [10, 23, 24, 26, 27, 30, 31, 77]

$$\varepsilon_H = -\frac{\dot{H}}{H^2}, \quad (15)$$

and

$$\eta_H = -\frac{\ddot{\phi}}{H\dot{\phi}}, \quad (16)$$

combined with the approximations  $\varepsilon_V \approx \varepsilon_H$  and  $\eta_V \approx \varepsilon_H + \eta_H$  to reach  $\varepsilon_V$  and  $\eta_V$  [4, 10, 11, 23, 26, 27, 29–31, 37, 77]

$$\varepsilon_V = \frac{M_{\text{Pl}}^2}{2} \left(\frac{V'(\phi)}{V(\phi)}\right)^2 = \frac{M_{\text{Pl}}^2 N^2}{2} \left(\frac{\sin(N\phi) - 2\gamma \sin(2N\phi)}{-\cos(N\phi) + \gamma \cos(2N\phi)}\right)^2, \quad (17)$$

and

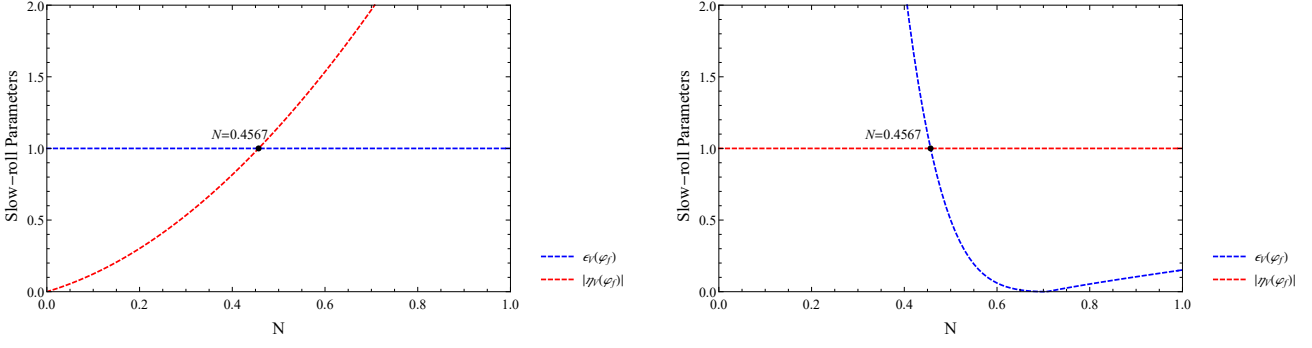


FIG. 3: Potential slow-roll parameters  $\varepsilon_V(\phi_f)$  and  $|\eta_V(\phi_f)|$  as functions of  $N$  for  $\alpha > 0$  and  $\gamma = -0.5$ . The condition for end of inflation in the interval  $N \leq 0.4567$  ( $N \geq 0.4567$ ) is  $\varepsilon_V(\phi_f) = 1$  ( $|\eta_V(\phi_f)| = 1$ ).

$$\eta_V = M_{\text{Pl}}^2 \frac{V''(\phi)}{V(\phi)} = M_{\text{Pl}}^2 N^2 \frac{\cos(N\phi) - 4\gamma \cos(2N\phi)}{-\cos(N\phi) + \gamma \cos(2N\phi)}, \quad (18)$$

called the potential slow-roll parameters. The slow-roll inflation requires  $\varepsilon_H, |\eta_H| \ll 1$  which also leads to  $\varepsilon_V, |\eta_V| \ll 1$  [10, 11, 23, 26, 27, 30, 31, 37, 77, 78]. The number of e-foldings is also calculated as [23, 24, 26, 27, 30, 31]

$$N_e = \int_{a_k}^{a_f} d \ln a = \int_{t_k}^{t_f} H dt, \quad (19)$$

which according to

$$H dt = \pm \frac{d\phi}{M_{\text{Pl}}} \frac{1}{\sqrt{2\varepsilon_V}}, \quad (20)$$

takes the form

$$\begin{aligned} N_e &= \frac{1}{M_{\text{Pl}}} \left| \int_{\phi_k}^{\phi_f} d\phi \frac{V(\phi)}{|V'(\phi)|} \right| \\ &= \left| \frac{1}{M_{\text{Pl}}^2 N^2 (-1 + 16\gamma^2)} \left[ \text{sign}(-\sin(N\phi_f) + 2\gamma \sin(2N\phi_f)) \right. \right. \\ &\quad \left. \left[ (1 + 8\gamma^2) \ln(|1 - 4\gamma \cos(N\phi_f)|) + 2(-1 - 3\gamma + 4\gamma^2) \right. \right. \\ &\quad \left. \left. \ln\left(\sin\left(\frac{N\phi_f}{2}\right)\right) + 2(-1 + 3\gamma + 4\gamma^2) \ln\left(\cos\left(\frac{N\phi_f}{2}\right)\right) \right] \right. \\ &\quad \left. - \text{sign}(-\sin(N\phi_k) + 2\gamma \sin(2N\phi_k)) \left[ (1 + 8\gamma^2) \right. \right. \\ &\quad \left. \left. \ln(|1 - 4\gamma \cos(N\phi_k)|) + 2(-1 - 3\gamma + 4\gamma^2) \ln\left(\sin\left(\frac{N\phi_k}{2}\right)\right) \right] \right. \\ &\quad \left. \left. + 2(-1 + 3\gamma + 4\gamma^2) \ln\left(\cos\left(\frac{N\phi_k}{2}\right)\right) \right] \right|. \end{aligned} \quad (21)$$

Here, the subscripts “k” and “f” refer to the Hubble horizon crossing and the end of inflation, respectively [27]. Note that  $\gamma = \pm 0.25$  leads to an infinite  $N_e$ , and are hence inappropriate.

Inflation ends when  $\phi_f$  meets the condition [26]

$$\max(\varepsilon_V(\phi_f), |\eta_V(\phi_f)|) = 1. \quad (22)$$

It is noteworthy that if  $\varepsilon_V$  ( $|\eta_V|$ ) touches one before  $|\eta_V|$  ( $\varepsilon_V$ ), then we have  $\varepsilon_V(\phi_f) = 1$  ( $|\eta_V(\phi_f)| = 1$ ) as the condition for reaching at the end of inflation. It should be noted that the two conditions can be satisfied simultaneously for some modified theories of gravity like Refs. [30, 31] and also  $V(\phi) \sim \phi^2$  in General Relativity (GR) [46]. Fig. 3 shows  $\varepsilon_V(\phi_f)$  and  $|\eta_V(\phi_f)|$  for  $\gamma = -0.5$ . The point  $N = 0.4567$  indicates a scenario where  $\varepsilon_V(\phi_f) = |\eta_V(\phi_f)| = 1$ . For  $N \leq 0.4567$  and  $N \geq 0.4567$ , inflation ends when  $\varepsilon_V(\phi_f) = 1$  and  $|\eta_V(\phi_f)| = 1$ , respectively.

The scalar spectral index  $n_s$  and the tensor-to-scalar ratio  $r$  are defined as [10, 24, 26, 27, 29–31, 37, 77]

$$\begin{aligned} n_s(\phi_k) &= 1 - 6\varepsilon_V(\phi_k) + 2\eta_V(\phi_k) \\ &= 1 - 3M_{\text{Pl}}^2 N^2 \left( \frac{\sin(N\phi_k) - 2\gamma \sin(2N\phi_k)}{-\cos(N\phi_k) + \gamma \cos(2N\phi_k)} \right)^2 \\ &\quad + 2M_{\text{Pl}}^2 N^2 \frac{\cos(N\phi_k) - 4\gamma \cos(2N\phi_k)}{-\cos(N\phi_k) + \gamma \cos(2N\phi_k)}, \end{aligned} \quad (23)$$

and

$$r = 16\varepsilon_V(\phi_k) = 8M_{\text{Pl}}^2 N^2 \left( \frac{\sin(N\phi_k) - 2\gamma \sin(2N\phi_k)}{-\cos(N\phi_k) + \gamma \cos(2N\phi_k)} \right)^2, \quad (24)$$

respectively. Using Eq. (23), one is able to find the possible values of  $\phi_k$  in the chosen interval  $0.92 \leq n_s \leq 1$ .

In order to find suitable ranges for the parameters  $N$  and  $\gamma$  generating acceptable inflation, one should pay attention to solving Eqs. (21) and (23) for all values of  $N$  and  $\gamma$  is impossible. Since a negative potential violates the slow-roll condition  $\dot{\phi}^2 \ll V(\phi)$  [10, 23, 26, 77], potential should be positive. We are also looking for realistic models satisfying the Planck 2018 data [1] and the Planck 2018 data+BK18+BAO [2]. Furthermore, we focus on  $N_e$  from 30 to 55 that is acceptable for solving

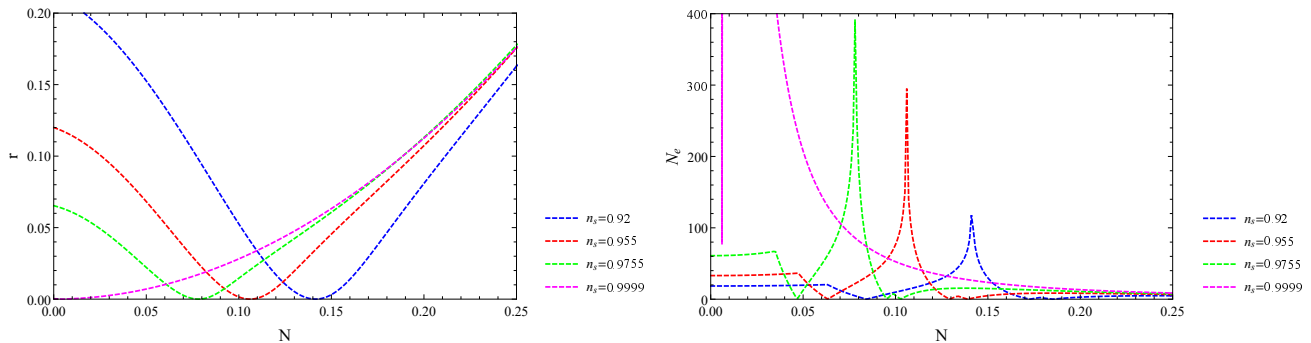


FIG. 4: Tensor-to-scalar ratio  $r$  and number of e-foldings  $N_e$  as functions of  $N$  for  $\alpha > 0$ ,  $\gamma = -0.5$  and four values of  $n_s$ . These plots play crucial roles in understanding the behaviors of  $r(n_s)$  and  $N_e(n_s)$ .

the problems of flatness, horizon, and magnetic monopole that meets the previous concerns [30, 31]. In addition, answers suggesting a contracting universe are unacceptable. In the following, we only focus on  $N > 0$ . However, the same results can be obtained by setting  $N < 0$  and converting  $\phi$  to  $-\phi$  because  $\cos(-x) = \cos(x)$ .

In Fig. 4,  $r(N)$  and  $N_e(N)$  are plotted for  $\alpha > 0$ ,  $\gamma = -0.5$  and four values of  $n_s$ .  $n_s = 0.955$  and  $n_s = 0.9755$  are of particular importance representing the approximate minimum and maximum permissible values of  $n_s$  based on the 95% CL of the Planck 2018 TT,TE,EE+lowE+lensing [1]. According to Fig. 4, the absolute minimum of  $r(N)$  and the absolute maximum of  $N_e(N)$  occur at the same  $N$ . These points with coordinates  $(N_m, r_{\min})$  and  $(N_m, N_{e,\max})$  play key roles in analyzing the behaviors of  $r(n_s)$  and  $N_e(n_s)$ . As  $n_s$  increases,  $r$  decrease (is enhanced) when  $N \leq N_m(n_s = 0.9999) = 0.005$  ( $N \geq N_m(n_s = 0.92) = 0.1411$ ). For  $0.005 < N < 0.1411$ , if point  $(n_{s,m}, r_{\min})$  is considered as the absolute minimum of  $r(n_s)$ , then the point  $(n_{s,m}, N_{e,\max})$  is the absolute maximum of  $N_e(n_s)$ . Additionally,  $r(n_s)$  is descending when  $0.92 \leq n_s < n_{s,m}$ , and is ascending when  $n_{s,m} < n_s \leq 1$ . As an example, for  $N = 0.1$ ,  $r(n_s)$  descends for  $0.92 \leq n_s < 0.96$  and ascends whenever  $0.96 < n_s \leq 1$ . If  $N$  is large enough, the  $r(N)$  curves for several values of  $n_s$  approach each other. In this situation, the rate of changes in  $N\phi_k$  for any  $n_s$  and  $N\phi_f$  with regard to  $N$  is almost constant. According to Eqs. (23) and (24), while  $r(N)$  grows in proportion to  $N^2$ ,  $r(n_s)$  is almost constant. According to the 95% CL of the Planck 2018 TT,TE,EE+lowE+lensing, the maximum acceptable value of  $r$  is 0.1295 [1], meaning that  $N > 0.2171$  is not allowed. Furthermore, as  $n_s$  is enhanced,  $N_e(n_s)$  increases when  $N > 0.1626$ . In the interval  $N < 0.1626$ , the behavior of  $N_e(n_s)$  has a strong dependence on the value of  $N$ . If  $N$  is large enough, the  $N_e(N)$  curves for different values of  $n_s$  approach each other. In this situation, according to Eqs. (21) and (23),  $N_e(N)$  decreases in proportion to  $\frac{1}{N^2}$ , while  $N_e(n_s)$  is nearly constant. In this paper, the minimum acceptable  $N_e$  is considered 30. Thus,  $N > 0.1415$  is not suitable as it cannot generate  $N_e > 30$ . The behaviors described by

$r(n_s)$  and  $N_e(n_s)$  can be traced in Figs. 5 and 6.

In the following, we focus on cases with satisfactory results. The solutions for Eq. (22) are found in the intervals 1 and 4 of Table I, indicating that the soliton field is positioned at the end of inflation in one of these intervals. If  $-1 < \gamma < 0$  and  $\gamma \geq 1$ , the initial soliton has a potential presence in four intervals of Table I, resulting in eight possible scenarios. However, if  $0 \leq \gamma < 1$ , the initial soliton can only be located in intervals 1 and 4, leading to four possible scenarios. Our analysis reveals that the results are inconsistent with the Planck 2018 data [1] and the Planck 2018 data+BK18+BAO [2] when  $\phi_k$  is located in the interval 3 of Table I at the beginning of inflation. Furthermore, there is no solution to Eq. (21) when inflation happens in the interval 1 of Table I. Scenarios stated in Table II can provide appropriate solutions, depending on the values of  $N$ ,  $\gamma$  and  $N_e$ . As an example, when  $\gamma = -0.5$ , Eq. (21) in case 3 does not produce solution for  $N_e = 30$  ( $N_e = 55$ ) within the range  $N > 0.074$  ( $N > 0.0547$ ). Indeed, there is only a solution for  $N = 10^{-4}$  in case 5.

In Fig. 5, the points  $(n_s, r)$  for  $N_e$  from 30 to 55 with a step range 5 and cases mentioned in Table II are shown. By increasing  $N_e$ , for each selected  $N$ ,  $r$  and  $n_s$  decrease in cases 1, 4 and 5 while  $r$  decreases (increases) and  $n_s$  increases(decreases) in case 2 (case 3). Furthermore, By increasing  $N$ , for each selected  $N_e$ ,  $n_s$  always decreases while  $r$  increases (decreases) in case 3 (case 5). In other cases, the behavior of  $r$  with respect to  $N$  changes in a specific  $N$ , which is denoted as  $N^*$  so that  $r$  increases (decreases) in the interval  $N < N^*$  ( $N > N^*$ ). The values of  $N^*$  for cases 1, 2 and 4 and  $N_e$  from 30 to 55 are mentioned in Table III. Another important point is the intersection of the  $r(N)$  for constant values of  $\gamma$  and  $N_e$  with 95% CL of the Planck 2018 data [1] yielding intervals of  $N$  in which the results can be compatible with the Planck 2018 data [1] and the Planck 2018 data+BK18+BAO [2], depending on the values of  $\gamma$  and  $N_e$ . Table IV lists these intervals of  $N$  for  $\gamma = -0.5$  and  $30 \leq N_e \leq 55$ .

So far, we have focused on  $\alpha > 0$  and  $\gamma = -0.5$ . Results show  $\alpha < 0$  leads to negative potential or imaginary solutions of Eqs. (21) and (23), which make it unaccept-

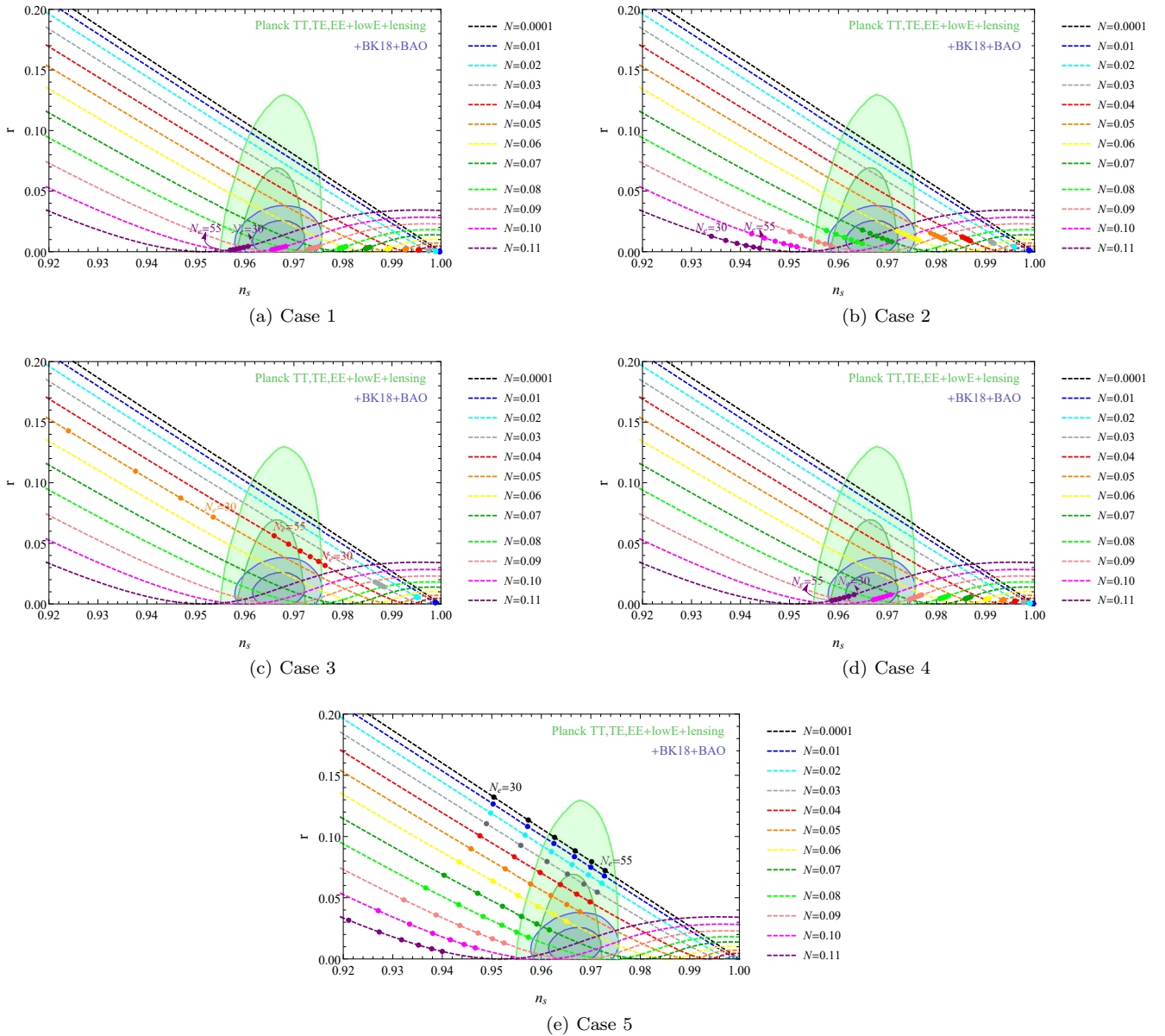


FIG. 5: Tensor-to-scalar ratio  $r$  as a function of  $n_s$  for cases mentioned on Table II,  $\alpha > 0$ ,  $\gamma = -0.5$  and several values of  $N$ . The 68% and 95% CL of the Planck 2018 TT,TE,EE+lowE+lensing (green contours) and the Planck 2018 TT,TE,EE+lowE+lensing+BK18+BAO (blue contours) are illustrated, such that the darker inner and lighter outer contours correspond to the 68% and 95% CL, respectively [1, 2]. Each  $r(n_s)$  curve shows the points  $(n_s, r)$  for the constant  $N_e$  ranging from 30 to 55. Note that in some cases, for certain values of  $N$ , these points are very close together. Furthermore, some of the points  $(n_s, r)$  in case 3 have  $n_s \leq 0.92$ , so they are not shown. When  $N > 0.1411$ ,  $r(n_s)$  increases, but decreases when  $N < 0.005$ . The point  $(n_{s,m}, r_{\min})$  represents the absolute minimum of  $r(n_s)$ . For  $0.005 < N < 0.1411$ ,  $r(n_s)$  decreases for  $0.92 \leq n_s < n_{s,m}$  and increases for  $n_{s,m} < n_s \leq 1$ . Eqs. (23) and (24) demonstrate that when  $N$  is sufficiently large,  $r(n_s)$  remains almost constant. The Planck 2018 TT,TE,EE+lowE+lensing measurements indicate that the maximum permissible value of  $r$  is 0.1295 [1], hence  $N > 0.2171$  is not permitted. When  $N_e$  increases for a selected  $N$ ,  $r$  and  $n_s$  both decrease in cases 1, 4, and 5, while in case 2 (case 3),  $r$  decreases (increases) and  $n_s$  increases (decreases). Furthermore, increasing  $N$  for a selected  $N_e$  always results in a decrease in  $n_s$ , while  $r$  increases (decreases) in case 3 (case 5). In the other cases, the behavior of  $r$  with respect to  $N$  changes at a specific  $N$ , denoted as  $N^*$ , where  $r$  increases when  $N < N^*$  and decreases when  $N > N^*$ . The values of  $N^*$  for cases 1, 2, and 4 and  $N_e$  ranging from 30 to 55 with a step size 5 are provided in Table III. Additionally, the intersection of  $r(N)$  for constant  $N_e$  with the 95% CL from the Planck 2018 data [1] provides intervals of  $N$  that may be consistent with the Planck 2018 data [1] and the Planck 2018 data+BK18+BAO [2], as shown in Table IV.

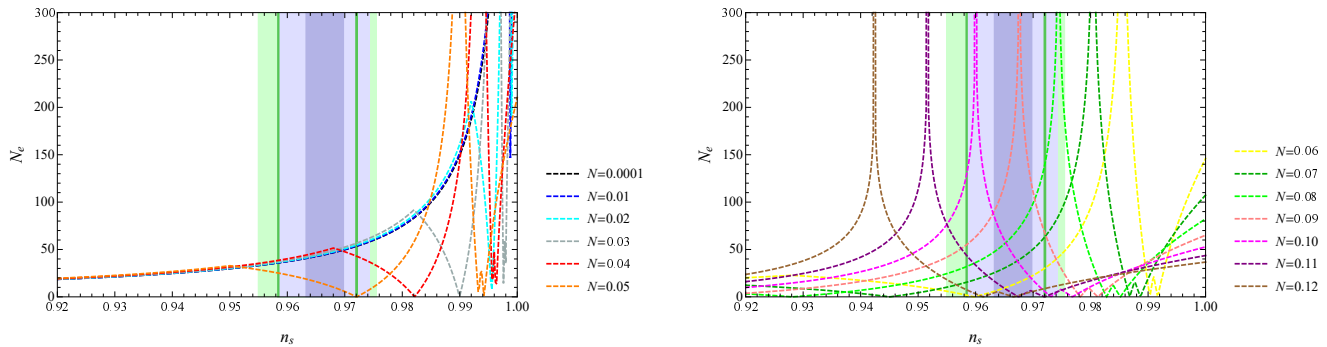


FIG. 6: Number of e-foldings  $N_e$  as function of  $n_s$  for the DSG potential (1),  $\alpha > 0$ ,  $\gamma = -0.5$  and several values of  $N$ . The green and blue regions represent the permissible ranges of  $n_s$  based on the Planck 2018 data [1] and the Planck 2018 data+BK18+BAO [2], respectively. The 68% regions are highlighted compared to the 95% regions [1, 2]. When  $n_s$  increases,  $N_e(n_s)$  increases for  $N > 0.1626$ , but for  $N < 0.1626$ ,  $N$  has a considerable influence on how  $N_e(n_s)$  behaves. If  $N$  is sufficiently large,  $N_e(n_s)$  approaches the constant value. In this paper, the minimum allowed  $N_e$  is 30. Consequently,  $N > 0.1415$  is invalid since it cannot result in  $N_e > 30$ .

Case	Interval of $N\phi_k$	Interval of $N\phi_f$
1	2	1
2	4	1
3	1	4
4	2	4
5	4	4

TABLE II: Cases that can produce results consistent with the Planck 2018 data [1] and the Planck 2018 data+BK18+BAO [2]. When  $\phi_k$  is in interval 3 of Table I, the results do not agree with the Planck 2018 data [1] and the Planck 2018 data+BK18+BAO [2]. In addition, when inflation takes place within interval 1 of Table I, there is no solution to Eq. (21).

$N_e$	$N^*$ for		
	Case 1	Case 2	Case 4
30	0.1033	0.0711	0.1064
35	0.0956	0.0658	0.0986
40	0.0894	0.0615	0.0923
45	0.0842	0.058	0.087
50	0.0799	0.055	0.0826
55	0.0762	0.0524	0.0787

TABLE III: The values of  $N^*$  for cases 1, 2 and 4 and  $N_e$  from 30 to 55.  $r$  increases in the interval  $N < N^*$  while it decreases in the  $N > N^*$ .

able. For the same reasons,  $\gamma < -1$  is also undesirable. Now, we intend to investigate how changes in  $\gamma$  affect the points  $(n_s, r)$  in Fig. 5. For this purpose,  $r(\gamma)$  and  $n_s(\gamma)$  have been depicted in Fig. 7. The study indicates that in cases 2, 3 and 5, suitable solutions may be obtained for  $\gamma > -1$ . For cases 1 and 4 the range  $-1 < \gamma < -0.25$  is acceptable because  $\gamma > -0.25$  results in negative po-

tential or imaginary solutions of Eqs. (21) and (23). As can be inferred from Fig. 7 the rate of changes in  $r$  and  $n_s$  increases with  $\gamma$  by increasing  $N$ . It is because for small values of  $N$ , such as  $N = 0.01$ ,  $\varepsilon_V$  and  $\eta_V$ , and consequently  $r$ ,  $n_s$ , and  $N_e$  are almost independent of  $\gamma$ . Moreover, as  $\gamma$  increases,  $r(\gamma)$  and  $n_s(\gamma)$  gradually converge to constant values. Another important point is that denoting the intersection of  $r(n_s)$  curves for constant  $N_e$  and  $N$  with 95% CL of the Planck 2018 data [1] provides intervals of  $\gamma$  in which the results can be compatible with the Planck 2018 data [1] and the Planck 2018 data+BK18+BAO [2], depending on the values of  $N_e$  and  $N$ . In Table V, these ranges of  $\gamma$  are specified for different cases mentioned in Table II.

#### IV. REHEATING

This section focuses on the reheating era by studying  $N_{\text{reh}}$  and  $T_{\text{reh}}$  [28, 29, 31, 36, 37]. In this regard, according to the Bianchi identity ( $G_{\mu\nu}^{\mu} = 0$ ), we have

$$\dot{\rho} + 3H(\rho + p) = 0, \quad (25)$$

combined with  $\omega = \frac{p}{\rho}$  to reach at

$$\rho = \rho_0 a^{-3(1+\omega)}. \quad (26)$$

Here,  $\omega$  is constant and the subscript 0 is related to present time. Eq. (27) displays the relationship between the energy density and the scale factor during reheating as

$$\frac{\rho_{\text{reh}}}{\rho_f} = \left(\frac{a_{\text{reh}}}{a_f}\right)^{-3(1+\omega_{\text{reh}})}. \quad (27)$$

The relationship between the values of scale factor at the end of inflation ( $a_f$ ), reheating ( $a_{\text{reh}}$ ), and the reheating number of e-foldings ( $N_{\text{reh}}$ ) is

$N_e$	Interval of $N$	$\omega_{\text{reh}} = -\frac{1}{3}$		$\omega_{\text{reh}} = -\frac{1}{6}$		$\omega_{\text{reh}} = 0$		$\omega_{\text{reh}} = \frac{1}{6}$	
		$N_{\text{reh}}$	$\log_{10}(\frac{T_{\text{reh}}}{\text{GeV}})$	$N_{\text{reh}}$	$\log_{10}(\frac{T_{\text{reh}}}{\text{GeV}})$	$N_{\text{reh}}$	$\log_{10}(\frac{T_{\text{reh}}}{\text{GeV}})$	$N_{\text{reh}}$	$\log_{10}(\frac{T_{\text{reh}}}{\text{GeV}})$
Case 1									
30	[0.0890,0.1165]	[51.68,51.80]	[4.12,4.17]	[68.91,69.06]	[-3.37,-3.30]	[103.36,103.6]	[-18.37,-18.27]	[206.73,207.20]	[-63.36,-63.16]
35	[0.0883,0.1154]	[41.57,41.74]	[6.28,6.34]	[55.42,55.65]	[0.24,0.32]	[83.14,83.48]	[-11.8393,-11.71]	[166.28,166.97]	[-48.09,-47.81]
40	[0.0876,0.1145]	[31.48,31.68]	[8.45,8.51]	[41.97,42.25]	[3.87,3.95]	[62.96,63.37]	[-5.30,-5.15]	[125.92,126.75]	[-32.82,-32.50]
45	[0.0871,0.1136]	[21.37,21.63]	[10.62,10.68]	[28.50,28.84]	[7.49,7.58]	[42.75,43.26]	[1.23,1.39]	[85.51,86.52]	[-17.55,-17.17]
50	[0.0865,0.1129]	[11.27,11.57]	[12.79,12.85]	[15.03,15.43]	[11.12,11.21]	[22.55,23.15]	[7.77,7.95]	[45.11,46.30]	[-2.28,-1.84]
55	[0.0860,0.1122]	[1.17,1.52]	[14.96,15.02]	[1.57,2.02]	[14.7481,14.85]	[2.35,3.04]	[14.30,14.50]	[4.71,6.08]	[12.98,13.48]
Case 2									
30	[0.0549,0.0829]	[52.48,52.63]	[4.03,4.11]	[69.98,70.17]	[-3.57,-3.48]	[104.97,105.26]	[-18.81,-18.68]	[209.94,210.52]	[-64.53,-64.26]
35	[0.0563,0.0860]	[42.35,42.57]	[6.21,6.28]	[56.47,56.76]	[0.05,0.15]	[84.71,85.15]	[-12.27,-12.10]	[169.42,170.30]	[-49.25,-48.89]
40	[0.0577,0.0888]	[32.21,32.51]	[8.38,8.46]	[42.95,43.35]	[3.68,3.80]	[64.43,65.03]	[-5.73,-5.52]	[128.87,130.06]	[-33.97,-33.51]
45	[0.0591,0.0911]	[22.07,22.45]	[10.56,10.64]	[29.43,29.93]	[7.31,7.44]	[44.15,44.90]	[0.80,1.05]	[88.31,89.81]	[-18.69,-18.12]
50	[0.0604,0.0932]	[11.93,12.38]	[12.73,12.81]	[15.91,16.51]	[10.94,11.08]	[23.87,24.77]	[7.35,7.63]	[47.75,49.55]	[-3.40,-2.73]
55	[0.0617,0.0949]	[1.79,2.32]	[14.90,14.98]	[2.39,3.09]	[14.57,14.72]	[3.59,4.64]	[13.90,14.72]	[7.18,9.28]	[11.88,12.64]
Case 3									
30	[0.0405,0.0485]	[53.03,53.23]	[4.01,4.06]	[70.70,70.97]	[-3.66,-3.63]	[106.06,106.46]	[-19.01,-19.05]	[212.12,212.93]	[-65.28,-65.07]
35	[0.0397,0.0469]	[43.04,43.25]	[6.18,6.23]	[57.39,57.672]	[-0.04,-0.02]	[86.09,86.50]	[-12.54,-12.50]	[172.19,173.01]	[-50.11,-49.89]
40	[0.0388,0.0454]	[33.06,33.27]	[8.35,8.40]	[44.08,44.36]	[3.56,3.58]	[64.12,65.54]	[-6.04,-6.00]	[128.25,133.08]	[-34.93,-34.72]
45	[0.0380,0.0441]	[23.08,23.28]	[10.52,10.57]	[30.77,31.04]	[7.18,7.20]	[46.16,46.57]	[0.46,0.50]	[92.32,93.14]	[-19.76,-19.54]
50	[0.0373,0.0429]	[13.09,13.30]	[12.69,12.74]	[17.45,17.73]	[10.80,10.82]	[26.18,26.60]	[6.96,7.01]	[53.20,52.37]	[-4.58,-4.36]
55	[0.0366,0.0418]	[3.10,3.31]	[14.86,14.91]	[4.14,4.41]	[14.41,14.43]	[6.21,6.62]	[13.47,13.51]	[12.42,13.24]	[10.60,10.81]
Case 4									
30	[0.0924,0.1195]	[51.91,52.02]	[4.13,4.17]	[69.21,69.36]	[-3.39,-3.33]	[103.82,104.04]	[-18.46,-18.36]	[207.64,208.08]	[-63.64,-63.45]
35	[0.0915,0.1181]	[41.81,41.96]	[6.29,6.34]	[55.75,55.95]	[0.22,0.29]	[83.62,83.93]	[-11.92,-11.81]	[167.25,167.86]	[-48.37,-48.12]
40	[0.0906,0.1169]	[31.71,31.91]	[8.46,8.51]	[42.28,42.55]	[3.84,3.92]	[63.43,63.82]	[-5.39,-5.25]	[126.86,127.65]	[-33.10,-32.80]
45	[0.0898,0.1158]	[21.61,21.85]	[10.63,10.68]	[28.82,29.13]	[7.47,7.55]	[43.23,43.70]	[1.14,1.29]	[86.47,87.41]	[-17.83,-17.48]
50	[0.0890,0.1148]	[11.52,11.80]	[12.80,12.85]	[15.36,15.74]	[11.09,11.18]	[23.04,23.61]	[7.67,7.85]	[46.08,47.22]	[-2.57,-2.15]
55	[0.0884,0.1140]	[1.42,1.75]	[14.97,15.02]	[1.89,2.33]	[14.72,14.81]	[2.84,3.50]	[14.21,14.40]	[5.69,7.00]	[12.69,13.16]
Case 5									
40	(0,0.0495]	[33.22,33.59]	[8.35,8.41]	[44.29,44.79]	[3.48,3.60]	[66.44,67.19]	[-6.23,-6.01]	[132.88,134.38]	[-35.41,-34.87]
45	(0,0.0694]	[22.88,23.56]	[10.50,10.60]	[30.50,31.42]	[7.09,7.29]	[45.76,47.13]	[0.27,0.67]	[91.52,94.26]	[-20.19,-19.20]
50	(0,0.0785]	[12.63,13.54]	[12.66,12.79]	[16.85,18.05]	[10.70,10.96]	[25.27,27.08]	[6.78,7.30]	[50.55,54.16]	[-4.97,-3.67]
55	(0,0.0843]	[2.42,3.51]	[14.83,14.97]	[3.23,4.68]	[14.32,14.62]	[4.85,7.03]	[13.30,13.91]	[9.71,14.06]	[10.24,11.80]

TABLE IV: The ranges of  $N$  that are compatible with the 95% CL of the Planck 2018 TT,TE,EE+lowE+lensing [1] for cases in Table II and  $N_e$  from 30 to 55 with a step size 5. Therefore, considering Fig. 5, the compatibility of the model with the Planck 2018 data [1] and the Planck 2018 data+BK18+BAO [2] is traceable. According to Eq. (41),  $N_e \geq 56.74$  leads to  $N_{\text{reh}} < 0$ , thus the maximum value for  $N_e$  is considered 55. Intervals of  $N_{\text{reh}}$  and  $\log_{10}(\frac{T_{\text{reh}}}{\text{GeV}})$  are established for  $\omega_{\text{reh}}$  between  $-\frac{1}{3}$  and  $\frac{1}{6}$ , with a step size of  $\frac{1}{6}$ . Red-colored cells indicate states that violate the BBN criterion  $T_{\text{reh}} < 10^{-2}$  GeV. In the case 1, for  $N_e = 50$  and  $\omega_{\text{reh}} = \frac{1}{6}$ , which is marked with yellow cells in the table,  $T_{\text{reh}} > 10^{-2}$  GeV when  $0.105 \leq N \leq 0.1129$ . In this situation, the acceptable range for  $N_e$  is also equal to  $45.11 \leq N_e \leq 45.55$ . As it is obvious from the table, the changes of  $N_{\text{reh}}$  and  $T_{\text{reh}}$  with respect to  $N$  and  $\gamma$  are gradual and mainly controlled by the values of  $N_e$  and  $\omega_{\text{reh}}$ . As  $N_e$  increases,  $N_{\text{reh}}$  decreases and  $T_{\text{reh}}$  increases. Furthermore, when  $\omega_{\text{reh}}$  increases,  $T_{\text{reh}}$  decreases while  $N_{\text{reh}}$  increases.

$$N_{\text{reh}} = \ln\left(\frac{a_{\text{reh}}}{a_f}\right), \quad (28) \quad \rho_{\text{reh}} = \rho_f e^{-3(1+\omega_{\text{reh}})N_{\text{reh}}}. \quad (30)$$

combined with Eq. (27) to obtain

$$N_{\text{reh}} = \frac{1}{3(1+\omega_{\text{reh}})} \ln\left(\frac{\rho_f}{\rho_{\text{reh}}}\right), \quad (29)$$

which subsequently results in

$$\rho_f = \frac{3}{2}V(\phi_f). \quad (31)$$

At the end of inflation, we have  $\varepsilon_V = 1$  meaning that  $\dot{H} = -H^2$  and thus, the connection between  $\rho_f$  and  $V(\phi_f)$  can be achieved as



Moreover, the relationship between  $\rho_{\text{reh}}$  and  $T_{\text{reh}}$  takes the form

$$\rho_{\text{reh}} = \frac{\pi^2}{30} g_{\text{reh}} T_{\text{reh}}^4, \quad (32)$$

in which  $g_{\text{reh}}$  denotes the number of relativistic species at the end of reheating.  $T_{\text{reh}}$  is related to the current temperature of the universe  $T_0$  via

$$T_{\text{reh}} = T_0 \left( \frac{a_0}{a_{\text{reh}}} \right) \left( \frac{43}{11g_{\text{reh}}} \right)^{\frac{1}{3}}. \quad (33)$$

Here,

$$\frac{a_0}{a_{\text{reh}}} = \left( \frac{a_0 H_k}{k} \right) e^{-N_e} e^{-N_{\text{reh}}}, \quad (34)$$

where  $k = a_k H_k$ . Using Eqs. (30)-(34),  $N_{\text{reh}}$  is obtained as

$$N_{\text{reh}} = \frac{4}{3(1 + \omega_{\text{reh}})} \left[ \frac{1}{4} \ln \left( \frac{45}{\pi^2 g_{\text{reh}}} \right) + \frac{1}{4} \ln \left( \frac{V(\phi_f)}{H_k^4} \right) + \frac{1}{3} \ln \left( \frac{11g_{\text{reh}}}{43} \right) + \ln \left( \frac{k}{a_0 T_0} \right) + N_e + N_{\text{reh}} \right]. \quad (35)$$

Now, by substituting  $g_{\text{reh}} = 106.75$ ,  $\frac{k}{a_0} = 0.05 \text{ Mpc}^{-1}$ , and  $T_0 = 2.725 \text{ K}$  into Eq. (35) [28, 29, 36, 37],  $N_{\text{reh}}$  is finally simplified as

$$N_{\text{reh}} = \frac{4}{1 - 3\omega_{\text{reh}}} \left[ 61.6 - \frac{1}{4} \ln \left( \frac{V(\phi_f)}{H_k^4} \right) - N_e \right]. \quad (36)$$

Using  $r = 16\varepsilon_V$ , one reaches

$$H_k = M_{\text{Pl}} \frac{\pi \sqrt{r A_s}}{\sqrt{2}}, \quad (37)$$

in which  $A_s = 2.196 \times 10^{-9}$  [28, 29, 36, 37]. By employing Eqs. (30)-(32),  $T_{\text{reh}}$  emerges as

$$T_{\text{reh}} = \left( \frac{45}{\pi^2 g_{\text{reh}}} V(\phi_f) \right)^{0.25} \frac{e^{-3(1 + \omega_{\text{reh}})N_{\text{reh}}}}{4}. \quad (38)$$

Considering  $\varepsilon_V \ll 1$  during the primary inflationary era,  $V(\phi_k)$  is calculated as

$$V(\phi_k) = 3M_{\text{Pl}}^2 H_k^2, \quad (39)$$

which leads to

$$\begin{aligned} V(\phi_f) &= V(\phi_k) \frac{-\cos(N\phi_f) + \gamma \cos(2N\phi_f)}{-\cos(N\phi_k) + \gamma \cos(2N\phi_k)} \\ &= 3M_{\text{Pl}}^2 H_k^2 \frac{-\cos(N\phi_f) + \gamma \cos(2N\phi_f)}{-\cos(N\phi_k) + \gamma \cos(2N\phi_k)}. \end{aligned} \quad (40)$$

Using Eqs. (36)-(40), it is a matter of calculation to reach

$$N_{\text{reh}} = \frac{4}{1 - 3\omega_{\text{reh}}} \left[ 56.74 - \frac{1}{4} \ln \left( \frac{1 - \cos(N\phi_f) + \gamma \cos(2N\phi_f)}{r - \cos(N\phi_k) + \gamma \cos(2N\phi_k)} \right) - N_e \right], \quad (41)$$

and

$$T_{\text{reh}} = (1.48642 \times 10^{16} \text{ GeV}) \left( r \frac{-\cos(N\phi_f) + \gamma \cos(2N\phi_f)}{-\cos(N\phi_k) + \gamma \cos(2N\phi_k)} \right)^{0.25} \frac{e^{-3(1 + \omega_{\text{reh}})N_{\text{reh}}}}{4}. \quad (42)$$

Eq. (41) shows that for  $N_e \geq 56.74$ ,  $N_{\text{reh}} < 0$ , which is not acceptable. Furthermore,  $\omega = \frac{1}{3}$  yields an infinite  $N_{\text{reh}}$ .

We now examine how parameters  $N_{\text{reh}}$  and  $T_{\text{reh}}$  behave in the range  $-\frac{1}{3} \leq \omega_{\text{reh}} \leq \frac{1}{6}$  in relation to  $N_e$ ,  $\omega_{\text{reh}}$ ,  $N$ , and  $\gamma$ . Eqs. (41) and (42) show that increasing  $N_e$  decreases the value of  $N_{\text{reh}}$  while increases  $T_{\text{reh}}$ . On the other hand, by increasing  $\omega_{\text{reh}}$ , the value of  $N_{\text{reh}}$  increases and  $T_{\text{reh}}$  decreases. Furthermore, the changes in  $N_{\text{reh}}$  and  $T_{\text{reh}}$  compared to  $N$  and  $\gamma$  are very slow and primarily depend on  $N_e$  and  $\omega_{\text{reh}}$  because of the term

$$\left\langle \frac{1}{4} \ln \left( \frac{1 - \cos(N\phi_f) + \gamma \cos(2N\phi_f)}{r - \cos(N\phi_k) + \gamma \cos(2N\phi_k)} \right) \right\rangle$$

in Eq. (41) and the term

$$\left\langle \left( \frac{-\cos(N\phi_f) + \gamma \cos(2N\phi_f)}{-\cos(N\phi_k) + \gamma \cos(2N\phi_k)} \right)^{0.25} \right\rangle$$

in Eq. (42) are significantly smaller than the other terms and coefficients. Tables IV and V provide evidence of these relationships.  $N_{\text{reh}}$  and  $T_{\text{reh}}$  are specified in Table IV for  $\gamma = -0.5$  and Table V for constant values of  $N$  ranges.

## V. SUMMARY AND DISCUSSIONS

Despite the many successes of the Big Bang theory [3, 5], it suffers from challenges including the flatness [6, 7], horizon [13], and magnetic monopole problems [14]. These issues are assumed to be solvable (or at least relaxed) by using the inflation theory based on introducing high-energy inflaton fields [16–22]. In this regard, motivated by the properties of Soliton fields [47–53], various

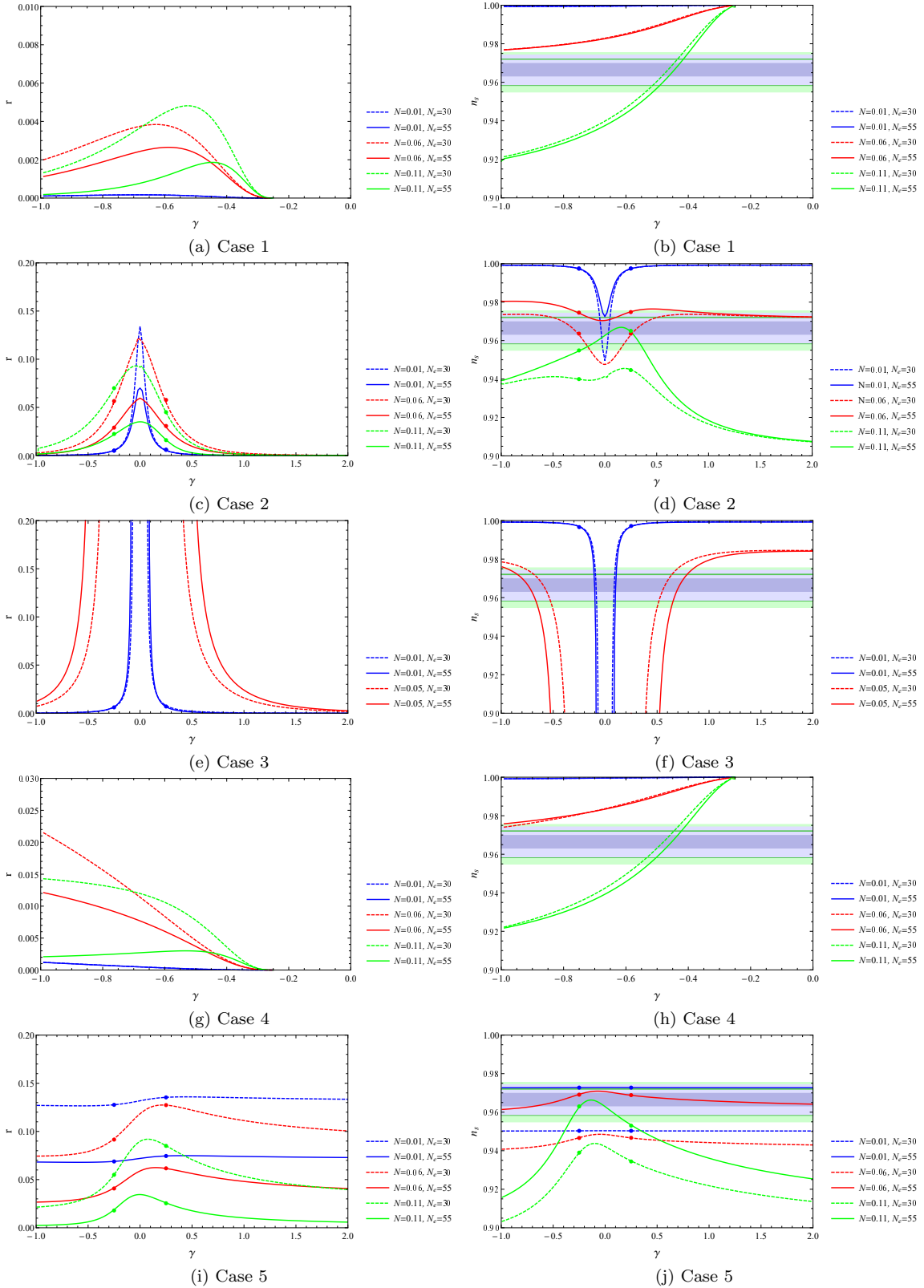


FIG. 7: Tensor-to-scalar ratio  $r$  and spectral index  $n_s$  as functions of  $\gamma$  for five cases presented in Table II,  $\alpha > 0$ , several values of  $N$ , as well as  $N_e = 30$  and  $N_e = 55$ . As mentioned earlier, for  $N > 0.0547$ , case 3 has a solution for  $N_e$  from 30 to 55. Therefore, plotting of  $r(\gamma)$  and  $n_s(\gamma)$  occurs for this example when  $N = 0.01$  and  $N = 0.05$ . The green and blue regions represent the permissible ranges of  $n_s$  based on the Planck 2018 data [1] and the Planck 2018 data+BK18+BAO [2], respectively. The 68% regions are highlighted compared to the 95% regions [1, 2]. In addition, bold points representing  $\gamma = \pm 0.25$  in accordance with Eq. (21), indicating the infinity of  $N_e$ , and are therefore unacceptable. As it is obvious from Fig. 7, solutions can be produced for  $\gamma > -1$  in cases 2, 3, and 5, while for cases 1 and 4, the range  $-1 < \gamma < -0.25$  is acceptable. In addition, the rate of change in  $r$  and  $n_s$  increases with  $\gamma$  as  $N$  increases. As  $\gamma$  increases,  $r(\gamma)$  and  $n_s(\gamma)$  increasingly approach constant values. The study lists intervals of  $\gamma$  that may correspond to the Planck 2018 data [1] and the Planck 2018 data+BK18+BAO [2] in Table V.

$N_e$	$N$	Interval of $\gamma$	$\omega_{\text{reh}} = -\frac{1}{3}$		$\omega_{\text{reh}} = -\frac{1}{6}$		$\omega_{\text{reh}} = 0$		$\omega_{\text{reh}} = \frac{1}{6}$	
			$N_{\text{reh}}$	$\log_{10}(\frac{T_{\text{reh}}}{\text{GeV}})$	$N_{\text{reh}}$	$\log_{10}(\frac{T_{\text{reh}}}{\text{GeV}})$	$N_{\text{reh}}$	$\log_{10}(\frac{T_{\text{reh}}}{\text{GeV}})$	$N_{\text{reh}}$	$\log_{10}(\frac{T_{\text{reh}}}{\text{GeV}})$
30	0.11	[-0.54,-0.42]	[51.6, 51.72]	[4.15,4.17]	[68.8,68.96]	[-3.222,-3.181]	[103.2,103.44]	[-18.3,-18.26]	[206.4,206.88]	[-63.22,-63.07]
55	0.11	[-0.51,-0.4]	[1.2,1.24]	[15,15.02]	[1.6,1.65]	[14.82,14.84]	[2.4,2.48]	[14.46,15]	[4.79,4.96]	[13.39,13.46]
Case 1										
30	0.01	[-0.03,0.03]	[53.598,53.608]	[4.012,4.014]	[71.46,71.48]	[-3.748,-3.744]	[107.2,107.22]	[-19.269,-19.263]	[214.39,214.43]	[-65.83,-65.82]
30	0.06	[-0.26,0.26]	[53.16,53.52]	[3.99,4.06]	[70.88,71.36]	[-3.76,-3.64]	[106.32,107.05]	[-19.26,-19.03]	[212.65,214.09]	[-65.74,-65.2]
55	0.01	[-0.023,0.023]	[3.49,4]	[14.822,14.824]	[4.65,4.66]	[14.315,14.319]	[6.97,6.99]	[13.303,13.309]	[13.95,13.99]	[10.27,9.486]
55	0.06	[-0.3,0.3]	[2.82,3.28]	[14.8,14.89]	[3.75,4.38]	[14.32,14.49]	[5.63,6.57]	[13.37,13.67]	[11.26,13.13]	[10.52, 11.22]
55	0.11	[-0.37,0.23]	[2.69,4.47]	[14.8,15]	[3.53,4.47]	[14.32,14.51]	[5.3,6.71]	[13.35,13.74]	[10.59,13.42]	[10.43,11.49]
Case 2										
30	0.01	[-0.096,-0.084]	[53.47,53.59]	[3.97,4.01]	[71.3,71.45]	[-3.77,-3.74]	[106.95,107.17]	[-19.257,-19.252]	[213.89,214.35]	[-65.8,-65.7]
30	0.01	[0.084,0.096]	[53.51,53.61]	[3.96,4]	[71.35,71.49]	[-3.78,-3.75]	[107.02,107.23]	[-19.277,-19.274]	[214.04,214.45]	[-65.84,-65.75]
30	0.05	[-0.79,-0.52]	[52.62,53.22]	[4.03,4.07]	[70.15,70.96]	[-3.63,-3.59]	[105.23,106.44]	[-19.04,-18.82]	[210.46,212.87]	[-65.26,-64.52]
30	0.05	[0.53,0.7]	[53.3,53.57]	[3.95,4]	[71.06,71.43]	[-3.76,-3.77]	[106.59,107.14]	[-19.27,-19.2]	[213.18,214.29]	[-65.8,-65.49]
55	0.01	[-0.108,-0.098]	[3.48,3.59]	[14.83,14.87]	[4.64,4.78]	[14.33,14.35]	[6.96,7.18]	[13.315,13.32]	[13.91,14.35]	[10.2,10.3]
55	0.01	[0.098,0.108]	[3.52,3.62]	[14.82,14.87]	[4.69,4.83]	[14.31,14.34]	[7.04,7.24]	[13.293,13.296]	[14.08,14.48]	[10.15,10.24]
55	0.05	[-0.97,-0.66]	[2.55,3.19]	[14.89,14.93]	[3.4,4.25]	[14.47,14.52]	[5.1,5.38]	[13.54,13.78]	[10.2,12.76]	[10.77,11.56]
55	0.05	[0.66,0.86]	[3.24,3.56]	[14.81,14.86]	[4.32,4.75]	[14.34,14.343]	[6.48,7.12]	[13.31,13.4]	[12.96,14.24]	[10.22,10.59]
Case 3										
30	0.11	[-0.56,-0.43]	[51.76,52.06]	[4.15,4.17]	[69.01,69.41]	[-3.34,-3.37]	[103.52,104.12]	[-18.44,-18.32]	[207.04,208.24]	[-63.66,-63.28]
55	0.11	[-0.52,-0.4]	[1.35,1.49]	[15,15.02]	[1.8,1.99]	[14.804,14.808]	[2.7,2.98]	[14.37,14.42]	[5.4,5.96]	[13.08,13.24]
Case 4										
55	0.01	$(-1, \infty)$	(3.5,4.85)	(14.4,14.83)	(4.67,6.47)	(13.7,14.33)	(7,9.7)	(12.29,13.31)	(14,19.41)	(8.07,10.27)
55	0.06	$(-1, \infty)$	(2.9,4.35)	(14.49,14.91)	(3.86,5.8)	(13.86,14.49)	(5.79,8.71)	(12.6,13.64)	(11.59,17.41)	(8.82,11.13)
55	0.11	[-0.34,0.18]	[4.13,4.88]	[15.17,15.42]	[5.5,6.51]	[14.58,14.72]	[8.25,9.76]	[13.3,13.38]	[16.511,19.52]	[9.07,9.8]
Case 5										

TABLE V: The ranges of  $\gamma$  that are compatible with the 95% CL of the Planck 2018 TT,TE,EE+lowE+lensing [1] for cases in Table II,  $N_e = 30$  and  $N_e = 55$ , as well as numerous values of  $N$ . Therefore, considering Fig. 7, the compatibility of the model with the Planck 2018 data [1] and the Planck 2018 data+BK18+BAO [2] is traceable. According to Eq. (41),  $N_e \geq 56.74$  leads to  $N_{\text{reh}} < 0$ , thus the maximum value for  $N_e$  is considered 55. For each of these ranges, intervals of  $N_{\text{reh}}$  and  $\log_{10}(\frac{T_{\text{reh}}}{\text{GeV}})$  are established for  $\omega_{\text{reh}}$  between  $-\frac{1}{3}$  and  $\frac{1}{6}$ , with a step size of  $\frac{1}{6}$ . Red-colored cells indicate states that violated the BBN criterion  $T_{\text{reh}} < 10^{-2}$  GeV. As it obvious from the table, the changes in  $N_{\text{reh}}$  and  $T_{\text{reh}}$  with respect to  $\gamma$  are gradual and mainly controlled by the values of  $N_e$  and  $\omega_{\text{reh}}$ . As  $N_e$  increases,  $N_{\text{reh}}$  decreases and  $T_{\text{reh}}$  increases. Furthermore, an increase in  $\omega_{\text{reh}}$  leads to an increase in  $N_{\text{reh}}$  and decrease in  $T_{\text{reh}}$ .

attempts have been followed by employing Soliton fields in studying inflation and early universe in various setups. However, despite the fact that reheating era plays a crucial role in connecting the achievements of inflation and Big Bang theories [25], there had not been a study on reheating for the DSG potential. Moreover, the consistency between solitonic potentials and observational data has only been examined for the PNGBs potential, using previous Planck data [59, 62]; hence, more recent research is required.

Here, considering DSG potential, we tried to provide a model for the early universe in agreement with the Planck 2018 data [1] and the Planck 2018 data+BK18+BAO [2]. The study shows that successful results require  $\alpha > 0$  and depend on the values of  $N$ ,  $\gamma$ , and  $N_e$ . Acceptable outcomes are found when  $-1 < \gamma < -0.25$  for cases 1 and 4,  $-1 < \gamma < 1$  for cases 2 and 3, and  $\gamma > -1$  for the fifth case. For example, the acceptable range of  $\gamma$  is  $-0.54 \leq \gamma \leq -0.42$  for case 1,  $N_e = 30$  and

$N = 0.11$ . Furthermore, range of  $N$  can be established for each  $\gamma$  and  $N_e$  in a consistent way with the Planck 2018 data [1] and the Planck 2018 data+BK18+BAO [2]. For instance, when  $\gamma = -0.5$ , valid solutions for  $r$  and  $n_s$  are limited to  $N < 0.1195$  that also depends on the studied case and the value of  $N_e$ . The reheating process was investigated by computing the parameters  $N_{\text{reh}}$  and  $T_{\text{reh}}$ . The results indicate that the dependence of  $N_{\text{reh}}$  and  $T_{\text{reh}}$  on the parameters  $N_e$  and  $\omega$ . Indeed,  $N_{\text{reh}}$  and  $T_{\text{reh}}$  progressively change with regard to  $N$  and  $\gamma$ . It is also obtained that solutions for  $N_e = 55$  are acceptable for the whole range of  $-\frac{1}{3} \leq \omega_{\text{reh}} \leq \frac{1}{6}$ . However, for  $N_e = 30$ , the range  $-\frac{1}{6} \leq \omega_{\text{reh}} \leq \frac{1}{6}$  is not allowed.

Investigating the consequences of modeling the early universe using other solitonic potentials is motivated by the current study. Moreover, providing solitonic models of various cosmic eras is helpful and can contribute to a broader knowledge of the evolution of the universe. Indeed, although the study of the slow-roll inflationary

scenario is crucial, it is just the starting point, and other scenarios such as constant-roll inflation [79–82] and warm inflation [83] are beneficial to be investigated. Furthermore, examining solitonic potentials within the framework of modified theories of gravity may yield valuable information about the early cosmos and the employed theory. Finally, it should be noted that analyzing the solitonic models by using the gravitational waves' data

such as NANOGrav [84–95] helps us obtain more appropriate models and indeed, has enough potential to be considered as future projects.

## ACKNOWLEDGMENTS

The work of KB was supported by the JSPS KAKENHI Grant Number 21K03547 and 24KF0100

- 
- [1] Y. Akrami *et al.*, *Astron. Astrophys.* **641**, A10(2020).  
 [2] P. A. R. Ade *et al.*, *Phys. Rev. Lett.* **127**, 151301 (2021).  
 [3] A. A. Penzias and R. W. Wilson, *Astrophys. J.* **142**, 419 (1965).  
 [4] G. Lazarides, *J. Phys. Conf. Ser.* **53**, 528 (2006).  
 [5] E. Hubble, *Proc. Natl. Acad. Sci.* **15**, 168 (1929).  
 [6] R. H. Dicke, *Gravitation and the Universe: Jayne Lectures for 1969*, American Philosophical Society, Philadelphia (1970).  
 [7] R. H. Dicke and P. J. E. Peebles, *The Big Bang Cosmology-Enigmas and Nostrums*. In: S. W. Hawking and W. Israel, *General Relativity: An Einstein Centenary Survey*, Cambridge University Press, Cambridge (1979).  
 [8] R. Brawer, *Inflationary Cosmology and Horizon and Flatness Problems: The Mutual Constitution of Explanation and Questions*, PhD thesis, Massachusetts Institute of Technology (1995).  
 [9] S. M. Carroll, arXiv:1406.3057 (2014).  
 [10] S. Zucchini, *Primordial Black Holes in String Inflation*, Master thesis, Alma Mater Studiorum Università di Bologna (2018).  
 [11] K. D. Lozanov, arxiv:1907.04402 (2019).  
 [12] P. Helbig *Mon. Not. R. Astron. Soc.* **495**, 3571 (2020).  
 [13] W. Rindler, *Mon. Not. R. Astron. Soc.* **116**, 662 (1956).  
 [14] P. A. M. Dirac, *Proc. Roy. Soc. Lond. A* **133**, 60 (1931).  
 [15] A. Rajantie, *Phil. Trans. R. Soc. A* **370**, 5705 (2012).  
 [16] A. H. Guth, *Phys. Rev. D* **23**, 347 (1981).  
 [17] A. A. Starobinsky, *Phys. Lett. B* **91**, 99 (1980).  
 [18] K. Sato, *Mon. Not. Roy. Astron. Soc.* **195**, 467 (1981).  
 [19] A. D. Linde, *Phys. Lett. B* **108**, 389 (1982).  
 [20] A. Albrecht and P. J. Steinhardt, *Phys. Rev. Lett.* **48**, 1220 (1982).  
 [21] S. W. Hawking, I. G. Moss and J. M. Stewart, *Phys. Rev. D* **26**, 2681 (1982).  
 [22] A. D. Linde, *Phys. Lett. B* **129**, 177 (1983).  
 [23] G. N. Remmen and S. M. Carroll, *Phys. Rev. D* **90**, 063517 (2014).  
 [24] Q. G. Huang, *J. Cosmol. Astropart. Phys.* **02**, 035 (2014).  
 [25] M. A. Amin, M. P. Hertzberg, D. I. Kaiser and J. Karouby, *Int. J. Mod. Phys.* **24**, 1530003 (2015).  
 [26] M. Amin, S. Khalil and M. Salah, *J. Cosmol. Astropart. Phys.* **08**, 043 (2016).  
 [27] C. Osses, N. Videla and G. Panotopoulos, *Eur. Phys. J. C* **81**, 485 (2021).  
 [28] F. S. Mirtalebian, K. Nozari and T. Azizi, *Astrophys. J.* **907**, 107 (2021).  
 [29] H. Zhou *et al.*, *Eur. Phys. J. C* **82**, 588 (2022).  
 [30] B. Afshar, N. Riazi and H. Moradpour, *Eur. Phys. J. C* **82**, 430 (2022).  
 [31] B. Afshar, H. Moradpour and H. Shabani, *Phys. Dark Univ.* **42**, 101357 (2023).  
 [32] S. Weinberg, *Cosmology*, Oxford University Press, New York (2008).  
 [33] S. D. Odintsov, V. K. Oikonomou, I. Giannakoudi, F. P. Fronimos and E. C. Lymperiadou, *Symmetry* **15**, no.9, 1701 (2023).  
 [34] A. R. Liddle and S. M. Leach, *Phys. Rev. D* **68**, 103503 (2003).  
 [35] R. Allahverdi, R. Brandenberger, F.-Y. Cyr-Racine and A. Mazumdar, *Annu. Rev. Nucl. Part. Sci.* **60**, 27 (2010).  
 [36] L. Dai, M. Kamionkowski and J. Wang, *Phys. Rev. Lett.* **113**, 041302 (2014).  
 [37] D. Y. Cheong, S. M. Lee and S. C. Park, *J. Cosmol. Astropart. Phys.* **02**, 029 (2022).  
 [38] I. D. Gialamas and A. B. Lahanas, *Phys. Rev. D* **101**, 084007 (2020).  
 [39] R. T. Co, E. Gonzalez and K. Harigaya, *J. Cosmol. Astropart. Phys.* **11**, 038 (2020).  
 [40] L. Ming, *Int. J. Mod. Phys. A* **36**, 2150170 (2021).  
 [41] J. D. Haro and L. A. Saló, *Phys. Rev. D* **107**, 063542 (2023).  
 [42] W. de Boer, *Prog. Part. Nucl. Phys.* **33**, 201 (1994).  
 [43] P. Saha, S. Anand and L. Sriramkumar, *Phys. Rev. D* **102**, 103511 (2020).  
 [44] A. Burgazlii, M. Eingorn and A. Zhuk, *Eur. Phys. J. C* **75**, 118 (2015).  
 [45] R. J. Nemiroff and B. Patla, *Am. J. Phys.* **76**, 265 (2008).  
 [46] D. Baumann, *Cosmology*, Cambridge University Press (2022).  
 [47] V. Mukhanov, *Physical Foundations of Cosmology*, Cambridge University Press, Cambridge (2005).  
 [48] M. P. Hobson, G. P. Efstathiou and A. N. Lasenby, *General Relativity, An Introduction for Physicists*, Cambridge University Press, Cambridge (2006).  
 [49] R. Durrer, *The Cosmic Microwave Background*, Cambridge University Press, Cambridge (2008).  
 [50] M. Roos, *Introduction to Cosmology*, John Wiley and Sons (2003).  
 [51] T. W. B. Kibble, *J. Phys. A: Math. Gen.* **9**, 1387 (1976).  
 [52] A. Vilenkin and E. P. S. Shellard, *Cosmic strings and other topological defects*, Cambridge University Press (1994).  
 [53] A. Riotto and M. Trodden, *Ann. Rev. Nuc. Part. Sci.* **49**, 35 (2002).  
 [54] K. Freese, J. A. Frieman, and A. V. Olinto, *Phys. Rev. Lett.* **65**, 3233 (1990).

- [55] K. Enqvist, S. Kasuya and A. Mazumdar, Phys. Rev. D **66**, 043505 (2002).
- [56] K. Freese and W. H. Kinney, Phys. Rev. D **70**, 083512 (2004).
- [57] P. Chen *et al.*, J. High Energy Phys. **0509**, 009 (2005).
- [58] K. T. Engel, Phys. Rev. D **81**, 12351 (2010).
- [59] K. Freese and W. H. Kinney, J. Cosmol. Astropart. Phys. **03**, 044 (2015).
- [60] E. W. Mielke, J. Phys.: Conf. Ser. **1208**, 012012 (2019).
- [61] J. I. Musmarra, M. Anabitarate and M. Bellini, Phys. Dark Univ. **24**, 10023 (2019).
- [62] E. W. Mielke, Phys. Lett. B **88**, 135538 (2020).
- [63] M. J. Duff, R. R. Khuri and J. X. Lu, Phys. Rept. **259**, 213 (1995).
- [64] M. Hamanaka, S. Huang and H. Kanno, Prog. Theor. Exp. Phys. **2023**, 043B03 (2023).
- [65] A. V. Grobov, A. E. Dmitriev, V. I. Dokuchaev and S. G. Rubin, Phys. Proc. **74**, 28 (2015).
- [66] Y. Bai, S. Lu and N. Orlofsky, J. High Energy Phys. **2022**, 181 (2022).
- [67] X. Du *et al.*, Phys. Rev. D **109**, 043019 (2024).
- [68] E. Franzin, M. Cadoni and M. Tuveri, Phys. Rev. D **97**, 124018 (2018).
- [69] G. Clément and A. Fabbri, Class. Quantum Grav. **17**, 2537 (2000).
- [70] E. Verdaguer, Phys. Rev. D **28**, 12 (1983).
- [71] D. Croon, A. Kusenko, A. Mazumdar and G. White, Phys. Rev. D **101**, 085010 (2020).
- [72] K. D. Lozanov, M. Sasaki and V. Takhistov, Phys. Lett. B **848**, 138392 (2024).
- [73] D. K. Campbell, M. Peyrard and P. Sodano, Physica D **19**, 165 (1986).
- [74] V. A. Gani and A. E. Kudryavtsev, Phys. Rev. E **60**, 3305 (1999).
- [75] T. Dauxios and M. Peyrard, *Physics of Solitons*, Cambridge University Press, Cambridge (2006).
- [76] N. R. Quintero, R. Alvarez-Nodarse and F. G. Mertens, Phys. Rev. E **80**, 016605 (2009).
- [77] Quintero et al. (2023) S. D. Odintsov *et al.*, Symmetry **15**, 1701 (2023).
- [78] S. Rasanen and E. Tomberg, J. Cosmol. Astropart. Phys. **01**, 038 (2019).
- [79] S. Inoue and J. Yokoyama, Phys. Lett. B **524**, 15 (2002).
- [80] M. H. Namjoo, H. Firouzjahi and M. Sasaki, Europhys. Lett. **101**, 39001 (2013).
- [81] J. Martin, H. Motohashi and T. Suyama, Phys. Rev. D **87**, 023514 (2013).
- [82] H. Motohashi, A. A. Starobinsky and J. Yokoyama, J. Cosmol. Astropart. Phys. **09**, 018 (2015).
- [83] A. Berera, Phys. Rev. Lett. **75**, 3218(1995).
- [84] S. Vagnozzi, Mon. Not. Roy. Astron. Soc. **502**, L11 (2021).
- [85] H. H. Li, G. Ye and Y. S. Piao, Phys. Lett. B **816**, 136211 (2021).
- [86] S. Kuroyanagi, T. Takahashi and S. Yokoyama, J. Cosmol. Astropart. Phys. **01**, 071 (2021).
- [87] Y. Cai and Y. S. Piao, Phys. Rev. D **103**, 083521 (2021).
- [88] B. Li and P. R. Shapiro, J. Cosmol. Astropart. Phys. **10**, 024 (2021).
- [89] M. Benetti, L. L. Graef and S. Vagnozzi, Phys. Rev. D **105**, 043520 (2022).
- [90] A. Ashoorioon, K. Rezazadeh and A. Rostami, Phys. Lett. B **835**, 137542 (2022).
- [91] S. Vagnozzi, arXiv:2306.16912 (2023).
- [92] J. Antoniadis *et al.* arXiv:2306.16227 (2023).
- [93] D. Borah, S. J. Das and R. Samanta, arXiv:2307.00537 (2023).
- [94] S. Datta, arXiv:2307.00646 (2023).
- [95] X. Niu and M. H. Rahat, arXiv:2307.01192 (2023).